ing time of large plutons. Figure 1b explores the influence of pluton size on the cooling history of a water-bearing granitic melt. Conduction cooling times vary with the square of R, whereas in convective cooling the solidification time varies approximately according to $R^{1.3}$ (Eq. 3).

Figure 2a shows the remarkable role water plays in determining the cooling time of granodioritic plutons. A pluton with 0.5 percent water (R = 5 km) cools to the solidus temperature in 330,000 years, whereas one with 4 percent water cools in only 50,000 years, other factors remaining constant. This is a graphic illustration of the importance of rheology in determining the thermal and chemical evolution of a magmatic system. For instance, mixing in a chemically (for example, water content) zoned magma chamber may be severely restricted due to a variation of an order of magnitude in the melt viscosity with depth. The influence of initial crystallinity and melt composition (excluding water) is summarized in Fig. 2b, where the thermal trajectories for granitic, granodioritic, and tonalitic plutons (R = 5 km) are given. The more mafic magmas have longer cooling histories because they are initially (that is, at $T = T_i$) partially crystallized and more viscous and consequently cool more slowly than related aphyric melts.

The parametric approach described here enables one to efficiently and simply evaluate the influence of various geometric, thermodynamic, thermophysical, and compositional factors on the cooling history of large volumes of magma emplaced within the crust. The calculations reported here are broadly compatible with the more detailed (in a spatial sense) and more laborious computations carried out by other works (*5*).

FRANK SPERA

Department of Geological and Geophysical Sciences, Princeton University, Princeton, New Jersey 08544

References and Notes

1. R. L. Smith and H. R. Shaw, *U.S. Geol. Surv. Circ. 726* (1975).
2. J. A. Whitney, *Econ. Geol.* **70**, 346 (1975); G. H. Brimhall, *ibid.* **72**, 37 (1977).
3. H. R. Shaw, in *Geochemical Transport and Kinetics*, A. Hofmann *et al.*, Eds. (Carnegie Institution of Washington, Washington, D.C., 1974), pp. 139–170; I. S. Carmichael, J. Nocholls, F. Spera, B. Wood, S. Nelson, *Philos. Trans. R. Soc. London Ser. A* **286**, 373 (1977).
4. An early example of a parameterized convection study is that of D. L. Turcotte and E. R. Oxburgh, *J. Fluid Mech.* **28**, 29 (1967). Other parametric studies of heat transfer and thermal convection include: R. W. Bartlett, *Am. J. Sci.* **267** (No. 3), 1067 (1969); B. D. Marsh, *Earth Planet. Sci. Lett.* **39**, 435 (1978); H. C. Hardee and D. W. Larson, *J. Volcanol. Geothermal Res.* **2**, 113 (1977).
5. D. S. Hodge, *Nature (London)* **251**, 297 (1974); H. R. Shaw, M. S. Hamilton, D. L. Peck, *Am. J. Sci.* **277** (No. 4), 384 (1977); D. L. Peck, M. S. Hamilton, H. R. Shaw, *ibid.*, p. 415.
6. H. R. Shaw, *Am. J. Sci.* **263**, 120 (1965); *J. Petrol.* **10**, 510 (1969); H. Pinkerton and R. S. Sparks, *Nature (London)* **276**, 383 (1978); S. A. F. Murrell and I. A. H. Ismail, *Contrib. Mineral. Petrol.* **55**, 317 (1976); C. Goetze, *J. Geophys. Res.* **76**, 1223 (1971).
7. The apparent viscosity is defined by the ratio $\sigma/\dot{\epsilon}$, where σ and $\dot{\epsilon}$ represent, respectively, the shear stress and strain rate of a single or multiphase fluid at a fixed temperature, pressure, and composition. The ratio $\sigma/\dot{\epsilon}$ is equal to the viscosity for a Newtonian fluid.
8. S. E. Swanson, *Am. Mineral.* **62**, 966 (1977); R. J. Kirkpatrick, *J. Geophys. Res.* **81**, 2565 (1976).
9. V. G. Levich, *Physiochemical Hydrodynamics* (Prentice-Hall, Englewood Cliffs, N.J., 1962); B. D. Marsh, *Trans. Am. Geophys. Union* **50**, 535 (1977).
10. Magma density, $\rho = 2.3$ g cm^{-3}; magma heat capacity, $C_p = 0.28$ cal g^{-1} sec^{-1}; thermal conductivity, $k = 5 \times 10^{-3}$ cal cm^{-1} sec^{-1} K^{-1}; contact temperature, T_c; heat of crystallization, ΔH = 80 cal g^{-1}; volume fraction of melt in the pluton, θ; temperature of the melt, T; time after the initiation of crystallization, t; isobaric expansivity, $\alpha = 5 \times 10^{-5}$ K^{-1}; acceleration, g = 981 cm sec^{-2}; kinematic viscosity at the liquidus temperature, $\nu_{T\ell}$; the viscosity parameter, $s = 0.08$, is defined by
$$\nu = \nu_{T_\ell} \ell^{s(T_\ell - T)};\ \kappa = \frac{k}{p_t C_p} = 10^{-2}\ \text{cm}^2\ \text{sec}^{-1}$$
T_ℓ, T_s, T_c, and T_i represent the melt liquidus, melt solidus, contact, and initial melt temperatures, respectively; p_t is pressure.
11. The definition of Ra appropriate to boundary layer thermal convection about a vertical pluton–country rock contact is
$$Ra = \frac{\alpha g (T - T_c) R^3}{\kappa \nu_{T_\ell}} \exp[s(T - T_\ell)]$$
This definition accounts for a strongly temperature-dependent magma viscosity.
12. For free convection about a vertical flat plate held at constant temperature, typical values are as follows: $a = 0.31$ and $b = 0.24$ (laminar flow); $a = 0.13$ and $b = 0.33$ (turbulent flow). Values for the uniform heat flux case are $a = 1.87$ and $b = 0.20$ (laminar flow). The boundary between turbulent and laminar convective flow regimes coincides roughly with $Ra = 10^{10}$ for high Prandtl number ($Pr = \nu/\kappa$) melts. In the numerical experiments reported here, $a = 0.305$ and $b = 0.239$. Data were compiled from W. M. Rohsenow and H. Y. Choi, *Heat, Mass, and Momentum Transfer* (Prentice-Hall, Englewood Cliffs, N.J., 1961); B. Gebhart, *J. Fluid Mech.* **14**, 225 (1962); K. Stewartson and L. T. Jones, *J. Aeronaut. Sci.* **24**, 379 (1957); M. J. Lighthill, *Q. J. Mech. Appl. Math.* **6** (Part 4), 399 (1953); R. Krishnamurti and F. B. Cheung, *Int. J. Heat Mass Transfer* **20**, 499 (1977).
13. J. C. Jaeger, in *The Poldervaart Treatise on Rocks of Basaltic Composition*, H. H. Hess and A. Poldervaart, Eds. (Interscience, New York, 1968), vol. 2, pp. 503–536; H. S. Carslaw and J. C. Jaeger, *Conduction of Heat in Solids* (Oxford Univ. Press, London, 1959).
14. J. L. Ahern, D. L. Turcotte, E. R. Oxburgh, *Trans. Am. Geophys. Union* **60**, 411 (1979).
15. J. K. Robertson and P. J. Wyllie, *J. Geol.* **79**, 549 (1971); J. A. Whitney, *ibid.* **83**, 1 (1975); H. R. Shaw, *Am. J. Sci.* **272**, 870 (1972); Y. Bottinga and D. R. Weill, *ibid.*, p. 438; H. R. Shaw, *J. Geophys. Res.* **68**, 6337 (1963); T. Murase and A. R. McBirney, *Geol. Soc. Am. Bull.* **84**, 3563 (1973).
16. Supported by NSF grant EAR 78-03340. I thank D. Yuen, G. Schubert, and L. Noodles for helpful discussion and motivation.

20 June 1979; revised 10 October 1979

Corotation Lag in Jupiter's Magnetosphere: Comparison of Observation and Theory

Abstract. *Voyager 1 plasma flow data are compared with a recent theory that predicted measurable departures from rigid corotation in Jupiter's magnetosphere as a consequence of rapid plasma production and weak atmosphere-magnetosphere coupling. The comparison indicates that the theory can account for the observed corotation lag, provided that the plasma mass production rate during the Voyager 1 encounter was rather larger than expected, namely ~ 10^{30} atomic mass units per second.*

Jupiter's magnetosphere contains prodigious sources of plasma, the most conspicuous being the innermost Galilean satellite Io (*1*). The magnetospheric plasma tends to corotate with the Jovian ionosphere, to which it is magnetically connected (barring large magnetic-field-aligned potential drops); thus the production and outward transport of magnetospheric plasma requires a net torque to transfer angular momentum outward from Jupiter's atmosphere to the magne-

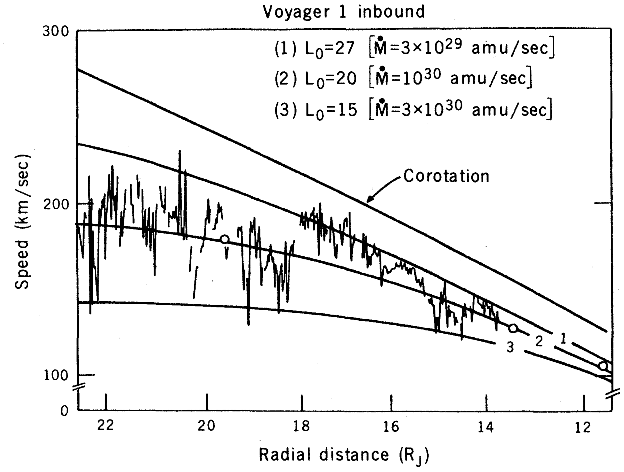

Fig. 1. Plasma rotational flow velocity as a function of radial distance in Jupiter's magnetosphere. The data (noisy curve plus circles) are reproduced from (*5*). The theoretical curves are derived from (*3*), with appropriate allowance made for the small but nonzero angle between the corotation direction and the viewing axis of the Voyager 1 instrument.

0036-8075/80/0118-0301$00.50/0

tospheric plasma (2). The application of this torque in turn requires that the ionosphere (and the magnetospheric flux tubes magnetically connected to the ionosphere) rotate somewhat slower than the neutral atmosphere.

A straightforward analysis of this coupling process (3) predicts a specific radial dependence of the required corotation lag, which becomes significant at distances of the order of L_0 R_J, with R_J = Jupiter radius and

$$L_0 = (\pi \Sigma R_J^2 B_J^2 / \dot{M})^{1/4}$$

where Σ is the effective height-integrated Pedersen conductivity of Jupiter's ionosphere, B_J is the dipole field strength at the surface, and $\dot{M}$ is the rate at which plasma mass is produced and transported outward in the magnetosphere. Pre-Voyager 1 estimates of Σ ($\sim$ 0.1 mho) and $\dot{M}$ ($\sim 10^{28}$ amu/sec) yielded the expected length scale $L_0 \sim 60$ (3).

The Voyager 1 plasma detector (4) has provided the first measurements of plasma flow in the Jovian magnetosphere. The results (5) are shown in Fig. 1. The departure from ideal corotation is seen to be significant as close in as $L \sim 10$. Figure 1 also shows theoretical curves derived directly from my earlier result (3) for three different values of L_0, corresponding to three possible values of the ratio $\Sigma/\dot{M}$. The large-scale radial dependence of the data is represented adequately for a value $L_0 \sim 20$.

Two interesting conclusions can be drawn from this comparison. First, it is qualitatively apparent that the atmosphere-magnetosphere coupling is indeed too weak to enforce corotation, a possibility that had been anticipated (2, 3) but not generally appreciated before Voyager 1 observations. Second, the comparison indicates that the pre-Voyager 1 estimate of L_0 ($\sim$ 60) was too large by a factor of 3, implying that the ratio $\Sigma/\dot{M}$ was, during the Voyager encounter, some two orders of magnitude smaller than anticipated. The pre-Voyager estimate of Σ ($\sim$ 0.1 mho) would appear, if anything, to be a lower limit because it is based on an ionosphere model that neglects the effects of auroral electron precipitation, which tends to increase the atmospheric conductivity (6). We are thus left with the conclusion that the mass-loading rate $\dot{M}$ was, during the Voyager 1 encounter, much larger than anticipated, namely, $\sim 10^{30}$ amu/sec (corresponding, for example, to 3×10^{28} S^+ ions per second. This exceeds by nearly an order of magnitude the S^+ injection rate suggested by Voyager 1 ultraviolet observations of the Io-associated plasma torus (7), which was itself much larger than had been anticipated. Recent analysis of Voyager 1 plasma data near Io's orbit tends to confirm the large mass-loading rate inferred above (8).

The large fluctuations of the data about the "average" ($L_0 = 20$) profile may be attributable to transient effects, inhomogeneities in Jupiter's ionospheric conductivity, localized convection cells, time variations in the mass-loading rate, and so forth. I will, however, follow the advice of the plasma experimenters that "structure in the curve should not be overinterpreted" (5).

T. W. HILL

Department of Space Physics and Astronomy, Rice University, Houston, Texas 77001

References and Notes

1. See, for example, G. L. Siscoe, *J. Geophys. Res.* **83**, 2118 (1978); T. W. Hill and F. C. Michel, *ibid.* **81**, 4561 (1976).
2. F. V. Coroniti, *Astrophys. J. Suppl. Ser.* **27**, 261 (1974); C. F. Kennel and F. V. Coroniti, *Space Sci. Rev.* **17**, 957 (1975); see also (3).
3. T. W. Hill, *J. Geophys. Res.* **84**, 6554 (1979).
4. H. S. Bridge *et al.*, *Science* **204**, 987 (1979).
5. R. L. McNutt, Jr., *et al.*, *Nature (London)* **280**, 803 (1979).
6. See, for example, A. J. Dessler and T. W. Hill, *Astrophys. J.* **227**, 664 (1979); see also (3).
7. A. L. Broadfoot *et al.*, *Science* **204**, 979 (1979).
8. G. L. Siscoe, personal communication.
9. A comparison similar to that made in this report was first presented by G. L. Siscoe (paper presented at the Magnetospheric Boundary Layer Conference, Alpbach, Austria, June, 1979). I am indebted to H. S. Bridge for furnishing a prepublication copy of the data shown in Fig. 1 and relevant details of the data analysis. I have enjoyed stimulating discussions on this subject with A. J. Dessler and G. L. Siscoe. Supported in part by NSF grant ATM78-21767.

28 August 1979

Net Energy Analysis of Alcohol Production from Sugarcane

Abstract. *Energy requirements were calculated for the agricultural and the industrial phase of ethyl alcohol production from sugarcane grown in Louisiana. Agricultural energy requirements comprised 54 percent of all energy inputs, with machinery, fuel, and nitrogen fertilizer representing most of the energy subsidies. Overall net energy benefits (output:input) for alcohol production ranged from 1.8:1 to 0.9:1 depending on whether crop residues or fossil fuels were used for industrial processes.*

In the search for alternative energy sources, considerable attention has been directed toward the production of alcohol to serve as a gasoline extender (gasohol) for internal combustion engines (1-4). Many gasoline retailers in the Midwest are already selling gasohol for use in automobiles (4). Although most industrial alcohol is produced from petroleum, most ethyl alcohol presently produced for blending with gasoline is based on agricultural crops as the raw material.

Table 1. Energetic cost of surgarcane production in Louisiana.

Input	Amount (per acre)	Energy expended ($\times 10^3$ kcal/ha)	Percent of total
Labor*	16.4 hours	22	0.3
Machinery†	$83	1576	18.6
Fuel‡	47 gal	4063	47.9
Nitrogen§	96 lb	1992	23.5
Phosphorus§	32 lb	120	1.4
Potassium§	48 lb	125	1.4
Seed‖	83,000 kcal	205	2.4
Insecticide¶	2.0 lb	54	0.6
Herbicide¶	10.6 lb	288	3.4
Total		8481	100

*From Campbell (11, 12); based on 8723 hours of labor per 675-acre farm plus one full-time manager at 45 hours per week; calorie equivalent, 544 kcal per man-hour (6). †From Campbell (11, 12), Pimentel *et al.* (6), and Ricaud (20); see (14) for explanation. ‡From Campbell (11, 12); includes transportation, tractors, harvesters, loaders, pickup trucks, and repair trucks; hours used times gallons per hour or miles per gallon; 35,000 kcal per gallon (22). §From Campbell (11, 12) and Carville (13); 120 lb of nitrogen, 40 lb of phosphorus, and 60 lb of potassium per acre planted. From Pimentel *et al.* (6) 8400, 1520, and 1050 kgal per pound for nitrogen, phosphorous, and potassium, respectively. ‖From Da Silva *et al.* (5); calorie equivalent of cane plant, 820,000 kcal/ha per 4 years. ¶From Campbell (11, 12) and Carville (13); 2.25 lb of insecticide per planted acre and 10.6 lb of herbicide applied per acre per year. From Pimentel *et al.* (6); 11,000 kcal per pound of insecticide or herbicide.

The gasohol production process needs to be thoroughly examined, however, before a large-scale production commitment is made in the United States. With the energy and land constraints that already exist for food production, it is important to analyze the net energy yield of alcohol production from agricultural crops, and to examine the consequences of the removal of significant portions of agricultural land from the food production base (5-9). In this report we analyze the net energy yield of fuel alcohol derived from sugarcane. The net energy analysis methodology presented here is adaptable to the analysis of other food (grain) crops and can therefore be used to make direct energy comparisons.

In modern agricultural systems, cultural energy subsidies have become integral and indispensable to the production process. In this study, direct energy (energy used for product manufacture as process heat) and material energy (capital equipment, services, labor input) subsidies to sugarcane were evaluated. Environmental inputs [rain, sun, wind, and soil; see Gilliland (10)] were not included, nor were federal, state, or local drainage project subsidies and costs of